A Geometric Method of Generalized Hoverability and Robustness Analysis for Marine Inspection UAVs

Abstract— **Close-proximity inspection of marine infrastructures requires UAVs to resist strong lateral sea breezes. To achieve the necessary decoupled control, multirotors with arbitrarily tilted rotors are increasingly deployed. However, existing geometric hoverability analyses assume strictly vertical rotors, rendering them mathematically invalid for the coupled 3D dynamics of generalized platforms. To address this, we mathematically decouple the full 6-DoF hovering equilibrium into internal moment balance and external force alignment. By introducing the *Generalized Moment Vector* (GMV), we prove a necessary and sufficient geometric condition: static hoverability requires the Center of Mass (CoM) to lie within the convex hull of the GMVs. Building on this criterion, we analytically construct the exact algebraic boundaries of the feasible CoM region. This method provides a deterministic design tool to evaluate asymmetric payload feasibility and rotor failure robustness, advancing the reliability of autonomous multirotors in high-risk offshore operations.**

I. INTRODUCTION

Aerial inspection of marine infrastructures requires UAVs to maintain stable proximity while resisting unpredictable lateral sea breezes. Standard planar quadrotors struggle here, as counteracting gusts requires pitching or rolling, which disrupts sensor targeting. Consequently, generalized multirotors with arbitrary rotor orientations are essential [1], [2], offering the decoupled 6-DoF actuation necessary for reliable marine operations.

However, evaluating the *static hoverability* of these generalized configurations is mathematically complex [3], [4], [6], [7], [8], [9], [10], [11], [13], [14]. While recent geometric methods elegantly determine the feasible Center of Mass (CoM) region by projecting the wrench space onto a 2D plane [5], [12], they strictly assume vertical rotor thrusts. In generalized marine platforms, arbitrarily tilted rotors induce coupled 3D forces and moments. This coupling renders existing planar geometric methods mathematically invalid.

To address this critical gap, we propose a rigorous geometric method for generalized hoverability analysis [5]. By mathematically decoupling the high-dimensional 6-DoF hovering equilibrium into *internal moment equilibrium* and *external force alignment*, we introduce the *Generalized Moment Vector* (GMV)—a unified descriptor aggregating each rotor's thrust, position, tilt, and drag. We prove that hoverability is geometrically equivalent to the CoM residing within the convex hull of the GMVs.

Building on this forward criterion, we develop an inverse geometric search algorithm that explicitly constructs the exact algebraic boundaries of the feasible CoM region using critical coplanar configurations of rotor triplets. This framework serves as a deterministic evaluation tool, enabling designers to rapidly assess CoM shifts caused by asymmetric marine payloads and quantitatively evaluate single-rotor failure robustness.

II. PRELIMINARIES AND PROBLEM FORMULATION

In this section, we extend the dynamical model presented in [5], which was originally limited to multirotors with strictly upward-oriented thrust, to encompass a generalized class of UAVs with arbitrary rotor positions and orientations for complex offshore tasks.

A. Generalized Dynamical Model

Let $\Sigma_o = \{O, \vec{e}_x, \vec{e}_y, \vec{e}_z\}$ be the inertial frame with gravity $\mathbf{g} = [0,0,-g]^\top$ (where $\vec{e}_z = [0,0,1]^\top$). The body-fixed frame $\Sigma_c = \{O_c, \vec{b}_x, \vec{b}_y, \vec{b}_z\}$ is attached to the vehicle's Center of Mass (CoM). The vehicle's configuration is defined by the CoM position $\mathbf{p} \in \mathbb{R}^3$ and attitude rotation matrix $\mathbf{R} \in SO(3)$, mapping Σ_c to Σ_o. The body angular velocity is denoted by $\boldsymbol{\omega} \in \mathbb{R}^3$.

Consider a UAV with n rotors. Rotor i ($i \in \{1,\dots,n\}$) is defined by its position $\mathbf{r}_i \in \mathbb{R}^3$ relative to the CoM and its orientation unit vector $\mathbf{n}_i \in \mathbb{R}^3$ ($||\mathbf{n}_i|| = 1$) in Σ_c. Unlike standard planar designs where $\mathbf{n}_i \equiv \vec{b}_z$, we allow arbitrary $\mathbf{n}_i$. Rotor i generates thrust $f_i \geq 0$ and drag torque $\tau_i = \kappa_i f_i$, yielding the CoM wrench:

$$\mathbf{F}_i = f_i \mathbf{n}_i, \quad \mathbf{M}_i = \mathbf{r}_i \times (f_i \mathbf{n}_i) + \kappa_i f_i \mathbf{n}_i \tag{1}$$

To facilitate our geometric approach, we factor out the scalar input f_i to define the *Generalized Moment Vector* (GMV), conceptually illustrated in :

Definition 1 (Generalized Moment Vector)**.** *The GMV* $\mathbf{m}_i \in \mathbb{R}^3$ *represents the total moment generated per unit of thrust for the i-th rotor:*

$$\mathbf{m}_i \triangleq \mathbf{r}_i \times \mathbf{n}_i + \kappa_i \mathbf{n}_i \tag{2}$$

Let $\mathbf{F}_c := [F_x\ F_y\ F_z\ M_x\ M_y\ M_z]^\top \in \mathbb{R}^6$ be the total wrench applied at the CoM. Stacking all n rotors yields:

$$\mathbf{F}_c = \begin{bmatrix} \mathbf{N} \\ \mathbf{M} \end{bmatrix} \mathbf{u} \tag{3}$$

where $\mathbf{N} = [\mathbf{n}_1, \dots, \mathbf{n}_n]$ and $\mathbf{M} = [\mathbf{m}_1, \dots, \mathbf{m}_n]$ are the force and moment distribution matrices, and $\mathbf{u} = [f_1, \dots, f_n]^\top$. In standard cases, $\mathbf{N}$ reduces to $[\mathbf{0}_{2\times n}; \mathbf{1}_{1\times n}]$, but in our generalized framework, $\mathbf{N}$ is fully populated.

The Newton-Euler dynamics are expressed as:

$$\begin{bmatrix} m\mathbf{I}_3 & \mathbf{O}_{3\times 3} \\ \mathbf{O}_{3\times 3} & \mathbf{J} \end{bmatrix} \begin{bmatrix} \dot{\mathbf{v}} \\ \dot{\boldsymbol{\omega}} \end{bmatrix} + \begin{bmatrix} \boldsymbol{\omega}^\wedge m\mathbf{v} \\ \boldsymbol{\omega}^\wedge \mathbf{J}\boldsymbol{\omega} \end{bmatrix} = \mathbf{F}_c - \begin{bmatrix} mg\mathbf{R}^\top \vec{e}_z \\ \mathbf{O}_{3\times 1} \end{bmatrix} \tag{4}$$

where m is the mass, $\mathbf{J}$ is the inertia matrix, and $(\cdot)^\wedge$ is the skew-symmetric operator.

To enable the decoupling analysis, we impose the following constraint:

Assumption 1 (Positive Lift Hypothesis)**.** *All rotor thrust directions satisfy* $\mathbf{n}_i \cdot \vec{b}_z > 0, \forall i$.

This ensures that any strictly positive input $\mathbf{u} > \mathbf{0}$ generates a net upward lift component, preventing degenerate solutions where opposing rotors cancel out thrust—a fundamental baseline for practical marine platforms.

B. Problem Formulation

For offshore inspections, maintaining a stable observation point is vital. *Static hovering* implies constant position and orientation ($\dot{\mathbf{v}} = \mathbf{0}$, $\dot{\omega} = \mathbf{0}$, and $\omega = \mathbf{0}$). Substituting these into (4) and using (3), the equilibrium becomes:

$$\mathbf{RNu} = mg\vec{e}_z, \quad \mathbf{Mu} = \mathbf{0} \tag{5}$$

Equation (5) represents external force balance and internal moment balance, respectively.

Definition 2 (Generalized Hoverability)**.** *A multirotor UAV is hoverable if there exist control input* $\mathbf{u} \in \mathbb{R}^n$ *and rotation matrix* $\mathbf{R} \in SO(3)$ *satisfying: (i) equilibrium equations (5); (ii) positivity constraint:* $\mathbf{u} > \mathbf{0}$*; (iii)* $rank(\mathbf{M}) = 3$ *(ensuring local controllability).*

Remark 1. *The strict positivity condition (*$\mathbf{u} > \mathbf{0}$*) provides a bidirectional control margin, which is essential for rejecting persistent lateral sea breezes.*

III. GENERALIZED HOVERABILITY ANALYSIS

Based on the dynamical model in Section II, we present the core theoretical framework. Static hoverability fundamentally requires finding a feasible equilibrium point in the high-dimensional coupled space $\mathcal{U} \times SO(3)$. Directly solving the nonlinear equations (5) is analytically intractable due to the non-convexity of $SO(3)$. To overcome this for complex marine UAV configurations, we propose a rigorous *decoupling strategy*.

A. Decoupling of Force and Moment Equilibrium

Let us define the force and moment generation maps, $\mathcal{F}(\mathbf{u}) = \mathbf{Nu}$ and $\mathcal{M}(\mathbf{u}) = \mathbf{Mu}$. The static hovering equilibrium condition (5) requires finding $\mathbf{u} \in \mathbb{R}^n$ and $\mathbf{R} \in SO(3)$ such that $\mathbf{R}\mathcal{F}(\mathbf{u}) = -m\mathbf{g}$ and $\mathcal{M}(\mathbf{u}) = \mathbf{0}$.

In standard planar multirotors, the net force direction is trivially invariant to $\mathbf{u}$. However, in generalized configurations designed for lateral wind rejection, the resultant force vector $\mathcal{F}(\mathbf{u})$ varies with $\mathbf{u}$, creating a bidirectional coupling. The following lemma resolves this, establishing that solving the moment equation is sufficient to guarantee a full 6-DoF equilibrium.

Lemma 1 (Decoupling and Existence)**.** *Consider a generalized multirotor UAV satisfying Assumption 1. The UAV is hoverable if and only if there exists a strictly positive input vector* $\mathbf{u}^* > \mathbf{0}$ *such that* $\mathbf{Mu}^* = \mathbf{0}$*, and the moment distribution matrix satisfies* $rank(\mathbf{M}) = 3$.

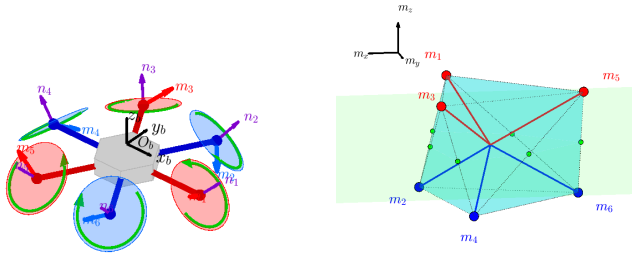

(a) (b)

Fig. 1: (a) A generalized multirotor UAV. (b) The 3D convex hull formed by the GMVs.

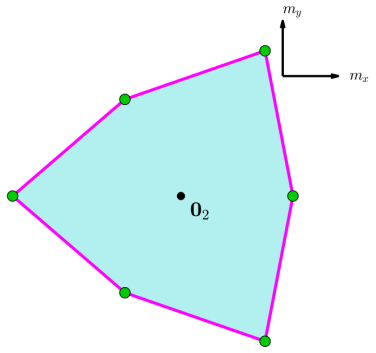

Fig. 2: 2D Generalized Hoverable Region $\mathcal{R}_{gen}$ (intersection of 3D polytope with $m_z = 0$). Hoverability requires $\mathbf{0}_2$ to be inside.

Proof. Necessity (⇒): If hoverable, there exists $(\mathbf{u}_{ss}, \mathbf{R}_{ss})$ satisfying equilibrium with $\mathbf{u}_{ss} > \mathbf{0}$. Thus, $\mathbf{u}^* = \mathbf{u}_{ss}$ satisfies $\mathbf{Mu}_{ss} = \mathbf{0}$. For local controllability (e.g., yaw authority against sea gusts), the block in the linearized dynamics dominated by $\mathbf{M}$ must have full rank, necessitating $\text{rank}(\mathbf{M}) = 3$.

Sufficiency (⇐): Suppose $\exists \mathbf{u}^* > \mathbf{0}$ satisfying $\mathbf{Mu}^* = \mathbf{0}$ with $\text{rank}(\mathbf{M}) = 3$. Let $\mathbf{F}^* = \mathcal{F}(\mathbf{u}^*) = \mathbf{Nu}^*$. Taking the inner product with the body z-axis yields $\mathbf{F}^* \cdot \vec{b}_z = \sum_{i=1}^n u_i^* (\mathbf{n}_i \cdot \vec{b}_z) > 0$ (by Assumption 1). This ensures $||\mathbf{F}^*|| > 0$. Defining a scalar gain $k = mg/||\mathbf{F}^*|| > 0$, the equilibrium input is $\mathbf{u}_{ss} = k\mathbf{u}^*$. Linearity ensures $\mathcal{M}(\mathbf{u}_{ss}) = \mathbf{0}$ and $\mathbf{u}_{ss} > \mathbf{0}$. Let $\hat{\mathbf{f}} = \mathbf{F}^*/||\mathbf{F}^*||$. We find $\mathbf{R}_{ss}$ such that $\mathbf{R}_{ss}\hat{\mathbf{f}} = \vec{e}_z$. One canonical solution via Rodrigues' formula is a rotation of angle $\theta = \arccos(\hat{\mathbf{f}} \cdot \vec{e}_z)$ about $\mathbf{k} = (\hat{\mathbf{f}} \times \vec{e}_z)/||\hat{\mathbf{f}} \times \vec{e}_z||$. Combined with $\text{rank}(\mathbf{M}) = 3$, this constructs a valid 6-DoF equilibrium. □

Remark 2. *If internal moments are balanced, the vehicle can hover at any desired heading angle. The rotation* $\mathbf{R}_{ss}$ *is determined only up to a rotation about gravity, meaning heading is structurally decoupled from hoverability.*

B. Forward Criterion via Virtual Equivalent Rotors

Checking Lemma 1 via 3D convex hull analysis offers little intuitive insight for marine UAV designers. To bridge this gap, we map the 3D GMVs $\mathbf{m}_i = [m_{ix}, m_{iy}, m_{iz}]^\top$ onto

a *Virtual Equivalent Rotor System*. We define virtual parameters: $\tilde{x}_i \triangleq -m_{iy}$, $\tilde{y}_i \triangleq m_{ix}$, and a generalized yaw capacity $\tilde{\kappa}_i \triangleq m_{iz}$.

We classify virtual rotors by their yaw capacity: $\mathcal{I}_+ = \{i \mid m_{iz} > 0\}$ and $\mathcal{I}_- = \{j \mid m_{jz} < 0\}$. For every pair $i \in \mathcal{I}_+, j \in \mathcal{I}_-$, we define a critical equilibrium point on the $m_z = 0$ plane:

$$\mathbf{d}_{ij} = \frac{-m_{jz}}{m_{iz} - m_{jz}} \begin{bmatrix} m_{ix} \\ m_{iy} \end{bmatrix} + \frac{m_{iz}}{m_{iz} - m_{jz}} \begin{bmatrix} m_{jx} \\ m_{jy} \end{bmatrix} \tag{6}$$

Let $\mathcal{D}$ be the set of all such points. The *Generalized Hoverable Region* $\mathcal{R}_{gen}$ is the 2D polygon $\text{Conv}(\mathcal{D})$ (Fig. 2).

Theorem 1 (Planar Reduction Criterion)**.** *A generalized multirotor is hoverable if and only if the origin* $\mathbf{0}_2$ *lies in the interior of the Generalized Hoverable Region:* $\mathbf{0}_2 \in int(\mathcal{R}_{gen})$.

Proof. By Lemma 1, hoverability is equivalent to $\mathbf{0}_3 \in \text{int}(\text{Conv}(\mathcal{M}))$. This 3D condition holds if and only if the slice of the moment polytope at $m_z = 0$ contains the origin. The set $\mathcal{D}$ represents exactly the vertices of this 2D slice, formed by combinations of positive and negative m_z vectors. Thus, checking $\mathbf{0}_2 \in \text{int}(\text{Conv}(\mathcal{D}))$ perfectly reduces the 3D verification to a 2D point-in-polygon test. □

C. Inverse Feasibility Region Generation for Marine Payloads

In marine inspections, mounting heavy asymmetric payloads (e.g., LiDAR, sub-sea sonars) causes significant CoM shifts $\mathbf{p} = [x, y, 0]^\top$. A critical design question is finding the *Feasible CoM Region* $\mathcal{D}_{CoM}$ where the UAV maintains omnidirectional moment authority.

With CoM shift $\mathbf{p}$, the GMV becomes affine: $\mathbf{m}_i(\mathbf{p}) = (\mathbf{r}_{i,0} - \mathbf{p}) \times \mathbf{n}_i + \kappa_i \mathbf{n}_i$. Consequently, the virtual rotors move and alter their yaw capacity dynamically. The boundary $\partial\mathcal{D}_{CoM}$ occurs when the origin $\mathbf{0}_2$ touches the boundary of the dynamic polygon $\mathcal{R}_{gen}(\mathbf{p})$. Mathematically, this singularity happens when a triplet of GMVs becomes coplanar with the origin:

$$\mathcal{C}_{ijk}(x, y) := \det([\mathbf{m}_i(\mathbf{p}), \mathbf{m}_j(\mathbf{p}), \mathbf{m}_k(\mathbf{p})]) = 0 \tag{7}$$

Expanding this determinant yields a *Cubic Algebraic Curve* $c_3x^3 + c_2x^2y + \cdots + c_0 = 0$. In standard planar quadrotors ($\mathbf{n}_i = \vec{b}_z$), cross-product terms cancel, degenerating the cubic curve into a straight line.

Instead of inefficient discrete sampling, the exact boundary $\partial\mathcal{D}_{CoM}$ is analytically generated by tracing the zero-level sets of $\mathcal{C}_{ijk}(x, y) = 0$ for all rotor triplets and filtering segments where $\mathbf{0}_2 \in \partial\mathcal{R}_{gen}(\mathbf{p})$ holds (Fig. 3).

Remark 3. *Unlike standard planar convex polygons, generalized regions bounded by cubic curves can be non-convex or even disconnected. This insight warns marine UAV designers against assuming simple convexity when evaluating payload distributions.*

IV. PERFORMANCE METRICS AND ROBUSTNESS

Beyond deterministic hoverability testing, our geometric framework provides continuous quantitative metrics to evaluate rotor-failure robustness and payload capacity. Both of these metrics are critical for ensuring the survivability of autonomous UAVs operating in harsh, unpredictable offshore environments.

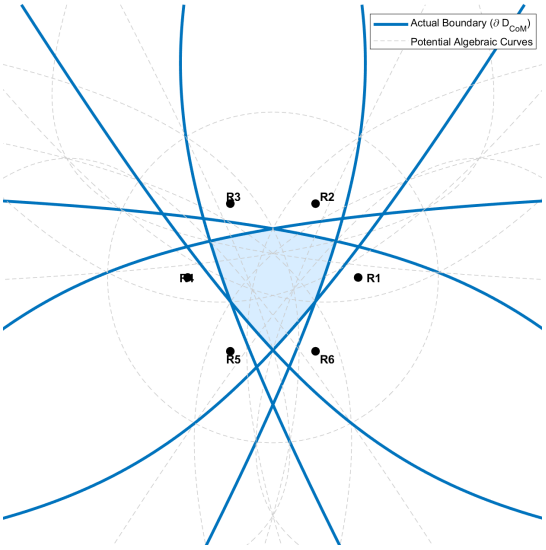

Fig. 3: Analytical determination of the feasible CoM region boundary. The blue curves represent zero-level sets of the cubic polynomials $\mathcal{C}_{ijk}(x, y) = 0$. The shaded interior delineates the safe payload distribution region.

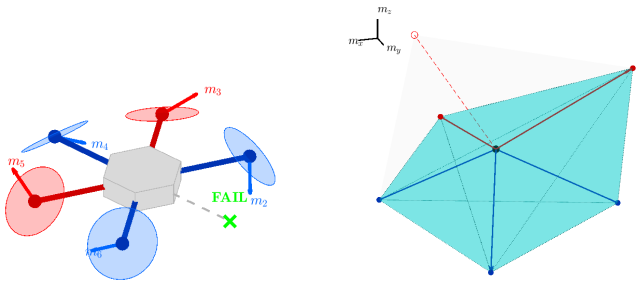

(a) (b)

Fig. 4: (a) Asymmetric configuration resulting from a single rotor failure ($u_k \equiv 0$). (b) Reduced 3D convex hull of the remaining GMVs; the system retains operational robustness if the origin remains strictly inside.

A. Generalized Rotor-Failure Robustness

In high-risk offshore operations, salt spray corrosion and bird strikes frequently cause sudden actuator failures. Standard fault-tolerance analyses, which rely on the rank of the control allocation matrix, often fail to account for the strictly positive thrust constraint ($u_i > 0$). Our geometric method inherently resolves this limitation via polytope convexity. A failure of rotor k ($u_k \equiv 0$) geometrically equates to removing its GMV $\mathbf{m}_k$ from the generating set $\mathcal{M}$ (Fig. 4).

Definition 3 (k-Loss Generalized Robustness)**.** *A multirotor UAV is robust to the failure of the k-th rotor if the origin remains strictly inside the reduced convex hull:*

$$\mathbf{0}_3 \in int(Conv(\mathcal{M} \setminus \{\mathbf{m}_k\})) \tag{8}$$

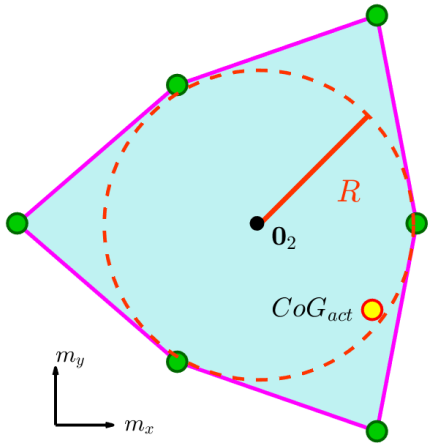

Fig. 5: Quantitative evaluation of the Hoverability Margin and the Maximum Inscribed Circle. CoG_{act} denotes the actual CoM position.

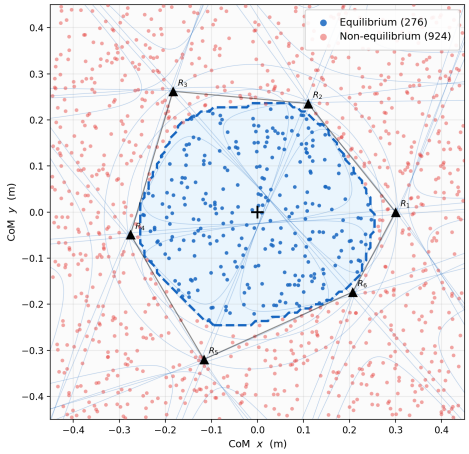

Fig. 6: Monte Carlo validation of the safe payload region. Blue dots denote hoverable CoM samples evaluated by Theorem 1; red dots denote catastrophic failures. The dashed blue curve is the exact analytical boundary $\partial\mathcal{D}_{\text{CoM}}$ computed via the cubic polynomials $\mathcal{C}_{ijk} = 0$.

This certification naturally extends to multiple simultaneous failures. Crucially, our 3D approach detects *coupled failure modes* that planar analyses inherently miss. For a tilted-rotor UAV facing sea breezes, losing a specific rotor might retain sufficient vertical lift but critically destroy the coupled lateral-yaw authority, making an emergency landing impossible. The 3D criterion rigorously captures these inter-axis couplings, ensuring full 6-DoF controllability recovery.

B. Quantitative Payload Margin Evaluation

Practical marine inspections require knowing how well a UAV can tolerate physical uncertainties. Mounting heavy, asymmetric payloadsunavoidably shifts the CoM $\mathbf{p}$. As illustrated in Fig. 5, we define the *Hoverability Margin* $\mu(\mathbf{p})$ as the minimum Euclidean distance from the actual CoM to the analytical cubic boundary $\partial\mathcal{D}_{CoM}$ derived in Section III-C. This metric exactly dictates the maximum allowable CoM shift before the UAV loses its omnidirectional gust resistance.

For robust platform design, maximizing the *Maximum Inscribed Circle Radius* $R_{ins} = \max_{\mathbf{p}} \mu(\mathbf{p})$ provides a powerful optimization objective. By treating the tilt angles $\mathbf{n}_i$ as decision variables, designers can synthesize non-intuitive, asymmetric configurations that significantly outperform standard layouts in both payload capacity and stability.

V. SIMULATION AND VALIDATION

To validate the proposed framework, we perform a Monte Carlo verification on a conceptual tilted-rotor marine hexarotor. The objective is to confirm that the analytically derived CoM boundaries—which represent the absolute safety limits for asymmetric payload shifts—are strictly consistent with the forward criterion established in Theorem 1.

The test platform (Table I) features an irregular placement with alternating 30° tangential tilts designed to provide decoupled lateral thrust against sea gusts. We first computed the exact boundary $\partial\mathcal{D}_{\text{CoM}}$ by tracing the zero-level sets of the polynomials $\mathcal{C}_{ijk}(x,y) = 0$. Subsequently, we uniformly sampled $1,200$ CoM positions across the domain—simulating extreme payload shifts—and evaluated Theorem 1 at each sample point.

TABLE I: Marine Inspection Hexarotor Configuration

Rotor	Position $\mathbf{r}_{i,0}^{\top}$ (m)	Orientation $\mathbf{n}_i^{\top}$	κ_i
R_1	(0.300, 0, 0)	(0, 0.50, 0.87)	+0.008
R_2	(0.110, 0.236, 0)	(0.45, −0.21, 0.87)	−0.008
R_3	(−0.184, 0.262, 0)	(−0.41, −0.29, 0.87)	+0.008
R_4	(−0.276, −0.049, 0)	(−0.09, 0.49, 0.87)	−0.008
R_5	(−0.116, −0.320, 0)	(0.47, −0.17, 0.87)	+0.008
R_6	(0.207, −0.174, 0)	(−0.32, −0.38, 0.87)	−0.008

As shown in Fig. 6, the analytical boundary perfectly separates the safe from unsafe payload distributions. Unlike standard planar quadrotors whose boundaries degenerate into straight lines, this generalized platform exhibits genuine cubic curvature arising from the coupled 3D rotor tilts. All 276 hoverable equilibrium points lie strictly inside the computed inverse region, while all non-equilibrium points lie outside. This confirms that the singularity condition $\det([\mathbf{m}_i, \mathbf{m}_j, \mathbf{m}_k]) = 0$ exactly and deterministically captures the physical hoverability limits of complex marine UAVs.

VI. CONCLUSION

This paper presented a rigorous geometric hoverability framework for marine UAVs with arbitrary rotor configurations. By introducing the Generalized Moment Vector (GMV) to decouple the 6-DoF equilibrium, we derived exact cubic CoM boundaries and a 2D geometric criterion, overcoming standard planar limitations. This deterministic tool enables rapid evaluation of asymmetric payloads and multi-rotor failure robustness under harsh maritime conditions. Ultimately, this foundation advances highly reliable, gust-resistant platforms for offshore inspections. Future work will integrate these boundaries into real-time, fault-tolerant control allocation.

REFERENCES

[1] G. Michieletto, M. Ryll and A. Franchi, "Control of statically hoverable multi-rotor aerial vehicles and application to rotor-failure robustness for hexarotors," in *Proc. IEEE Int. Conf. Robotics and Automation (ICRA)*, Singapore, 2017, pp. 2747–2752.

[2] M. Hamandi, Q. Sable, M. Tognon and A. Franchi, "Understanding the omnidirectional capability of a generic multi-rotor aerial vehicle," in *Proc. Aerial Robotic Systems Physically Interacting with the Environment (AIRPHARO)*, Biograd na Moru, Croatia, 2021, pp. 1–6.

[3] R. Murata, T. Urakubo, C. Kikumoto and K. Sabe, "Optimization of Thrust and Pitch Angle Allocation for a Dual-System VTOL UAV in Hover," in *Proc. 13th Int. Conf. Control, Mechatronics and Automation (ICCMA)*, Paris, France, 2025, pp. 312–317.

[4] H. Z. I. Khan, S. Mobeen, J. Rajput and J. Riaz, "Nonlinear Control Allocation: A Learning Based Approach," in *Proc. IEEE 63rd Conf. Decision and Control (CDC)*, Milan, Italy, 2024, pp. 2833–2838.

[5] S. Mochida, R. Matsuda, T. Ibuki and M. Sampei, "A Geometric Method of Hoverability Analysis for Multirotor UAVs With Upward-Oriented Rotors," *IEEE Trans. Robot.*, vol. 37, no. 5, pp. 1765–1779, 2021.

[6] G.-X. Du, Q. Quan, B. Yang and K.-Y. Cai, "Controllability analysis for multirotor helicopter rotor degradation and failure," *J. Guid., Control, Dyn.*, vol. 38, no. 5, pp. 978–985, 2015.

[7] K. Kim, S. Rahili, X. Shi, S.-J. Chung and M. Gharib, "Controllability and design of unmanned multirotor aircraft robust to rotor failure," in *Proc. AIAA Scitech 2019 Forum*, 2019, AIAA Paper 2019-1787.

[8] G. Michieletto, M. Ryll and A. Franchi, "Fundamental actuation properties of multirotors: Force-moment decoupling and fail-safe robustness," *IEEE Trans. Robot.*, vol. 34, no. 3, pp. 702–715, 2018.

[9] J. I. Giribet, R. S. Sanchez-Pena and A. S. Ghersin, "Analysis and design of a tilted rotor hexacopter for fault tolerance," *IEEE Trans. Aerosp. Electron. Syst.*, vol. 52, no. 4, pp. 1555–1567, 2016.

[10] D. Vey and J. Lunze, "Structural reconfigurability analysis of multirotor UAVs after actuator failures," in *Proc. 54th IEEE Conf. Decision and Control (CDC)*, 2015, pp. 5097–5104.

[11] M. W. Mueller and R. D'Andrea, "Stability and control of a quadrocopter despite the complete loss of one, two, or three propellers," in *Proc. IEEE Int. Conf. Robotics and Automation (ICRA)*, 2014, pp. 45–52.

[12] R. Matsuda, T. Ibuki, and M. Sampei, "A hoverability analysis method for multirotor UAVs with a case study on fault tolerance," in *Proc. 57th IEEE Conf. Decis. Control.*, 2018, pp. 4264–4269.

[13] X. Liang, Y. Fang, N. Sun, and H. Lin, "Nonlinear hierarchical control for unmanned quadrotor transportation systems," *IEEE Trans. Ind. Electron.*, vol. 65, no. 4, pp. 3395–3405, Apr. 2018.

[14] M. Orsag, C. Korpela, S. Bogdan, and P. Oh, "Dexterous aerial robots mobile manipulation using unmanned aerial systems," *IEEE Trans. Robot.*, vol. 33, no. 6, pp. 1453–1466, Dec. 2017.